

Positioning of Particles in Active Droplets

David Zwicker,^{1,2,3,*} Johannes Baumgart,³ Stefanie Redemann,^{4,5} Thomas Müller-Reichert,⁴
Anthony A. Hyman,⁶ and Frank Jülicher³

¹Max Planck Institute for Dynamics and Self-Organization, 37077 Göttingen, Germany

²John A. Paulson School of Engineering and Applied Sciences, Harvard University,
Cambridge, Massachusetts 02138, USA

³Max Planck Institute for the Physics of Complex Systems, 01187 Dresden, Germany

⁴Technische Universität Dresden, Experimental Center, Faculty of Medicine Carl Gustav Carus,
Fiedlerstraße 42, 01307 Dresden, Germany

⁵Center for Membrane and Cell Physiology and Department of Molecular Physiology and Biological Physics,
University of Virginia, School of Medicine, Charlottesville, Virginia 22903, USA

⁶Max Planck Institute of Molecular Cell Biology and Genetics, 01307 Dresden, Germany



(Received 16 March 2018; revised manuscript received 6 August 2018; published 12 October 2018)

Chemically active droplets are nonequilibrium systems that combine phase separation with chemical reactions. We here investigate how the activity introduced by the chemical reactions influences solid particles inside such droplets. We find that passive particles are centered in active droplets governed by first-order reactions. In autocatalytic active droplets, only catalytically active particles can be centered. An example of such systems in biology are centrosomes. Our study can account for the observed positioning of centrioles and provides a general mechanism to control the position of particles within chemically active droplets.

DOI: 10.1103/PhysRevLett.121.158102

Liquid droplets can be driven away from thermal equilibrium by chemical reactions that take place inside a droplet or in its environment. The combination of phase separation and chemical reactions generates dynamical features in such active droplets that do not occur in conventional passive droplets. For instance, Ostwald ripening can be suppressed [1], and droplets can divide spontaneously [2]. Examples for active droplets can be found in living cells, where the formation of dropletlike assemblies plays an important role in the spatial organization of chemical processes [3–7]. Since cellular processes are tightly controlled, studying such droplets can shed light on new physical mechanisms for controlling liquid droplets in nonequilibrium environments.

A particular interesting example of active droplets in cells are centrosomes [8]. A centrosome consists of a soft pericentriolar material (PCM) [9–12], which can be described as a droplet phase that grows via an autocatalytic chemical process [8,13]. This droplet phase is nucleated by the catalytic activity of a pair of centrioles. These are nanoscale structures that are embedded in the droplet material and are typically observed near the geometric center of the spherical centrosome. The control of nucleation by catalytically active centrioles ensures that mitotic cells possess exactly two centrosomes of similar size to organize the bipolar mitotic spindle [14]. These findings raise the question of what physical mechanisms govern the spatial organization of centrosomes and, more generally, how passive and active particles are positioned inside active droplets.

Here, we present a general physical mechanism for the positioning of particles inside active droplets. This positioning is mediated by nonequilibrium fluxes associated with chemical reactions. We base our study on the general theory of chemically active droplets that combines classical phase separation with reaction-diffusion systems. For simplicity, we consider a two-phase system that is sufficient to illustrate the general principles [1]. Chemical reactions induce transitions between two molecular species A and B that phase separate. The droplet is formed by a phase that is rich in B which coexists with a solvent phase characterized by high A concentration. Following our earlier approach [1,8], we denote by $\phi^A(\mathbf{r}, t)$ and $\phi^B(\mathbf{r}, t)$ the local volume fractions of A and B molecules, respectively. The remaining volume fraction of the solvent is thus $\phi^C = 1 - \phi^A - \phi^B$. In the bulk phases away from the interface, components diffuse and are converted into each other by chemical reactions [1]:

$$\partial_t \phi^A = D \nabla^2 \phi^A - k_{AB} \phi^A + k_{BA} \phi^B - k \phi^A \phi^B, \quad (1a)$$

$$\partial_t \phi^B = D \nabla^2 \phi^B + k_{AB} \phi^A - k_{BA} \phi^B + k \phi^A \phi^B. \quad (1b)$$

For simplicity, we here consider the case of equal diffusivity D for both components, and we express the reaction flux using the terms of lowest order: The first-order transitions are associated with rate constants k_{AB} and k_{BA} , and we also consider a second-order, autocatalytic reaction $A + B \rightarrow 2B$ with rate constant k , which is relevant for centrosomes [8].

In the biological context, reactions are typically subject to external energy input, and their rates thus do not obey detailed balance.

At the droplet interface, the chemical potentials of components A and B are continuous, and the pressure difference across the interface is given by the Laplace pressure γH , where γ denotes the surface tension and H is the local mean curvature of the interface. This provides conditions for the volume fractions ϕ^B inside and outside the droplet at the interface, which we denote ϕ_-^B and ϕ_+^B , respectively. They can be expressed as $\phi_{\pm}^B(\mathbf{R}) \approx \psi_{\pm} + \gamma\beta_{\pm}H(\mathbf{R})$ at the droplet interface located at position \mathbf{R} [8]. Here, ψ_- and ψ_+ denote the equilibrium volume fractions inside and outside of a flat interface, respectively, and the coefficients β_- and β_+ describe the influence of the Laplace pressure $2\gamma H$ on the equilibrium volume fractions. Note that typical droplets in biological cells are not very dense in droplet material and can even be porous, like centrosomes [15]. This implies that a large fraction of the droplet volume is occupied by other components, which we capture by considering $\psi_- = 0.1$. In our model, the droplet material B segregates from the precursors A and the solvent C , while A and C mix, so that the precursors are soluble in the solvent. This corresponds to the condition $\phi_+^A(\mathbf{R})/[1-\phi_+^B(\mathbf{R})] = \phi_-^A(\mathbf{R})/[1-\phi_-^B(\mathbf{R})]$. The local interface speed $v = \mathbf{n}(\mathbf{R}) \cdot \partial_t \mathbf{R}$ in its normal direction \mathbf{n} is related to the normal fluxes $j_{\pm}^i(\mathbf{R}) = \mathbf{n}(\mathbf{R}) \cdot \mathbf{j}_{\pm}^i(\mathbf{R})$, where $\mathbf{j}_{\pm}^i(\mathbf{R})$ and $\mathbf{j}_{\pm}^i(\mathbf{R})$ denote the diffusion fluxes $\mathbf{j}^i = -D\nabla\phi^i$ when approaching the interface from the inside and the outside, respectively. Material conservation implies the two conditions

$$v(\mathbf{R}) = \frac{j_-^i(\mathbf{R}) - j_+^i(\mathbf{R})}{\phi_-^i(\mathbf{R}) - \phi_+^i(\mathbf{R})} \quad (2)$$

for $i = A, B$.

A particle inside the droplet can contribute by its chemical activity. For instance, precursors A can be directly transformed to droplet material B by a first-order reaction $A \rightarrow B$ catalyzed at the particle surface, e.g., by centrioles in centrosomes [8]. We express the volume of droplet material B produced per unit area at the particle surface per unit time as $q_{AB}\phi^A(\mathbf{r}_a)$, where \mathbf{r}_a is a vector pointing at the particle surface and the parameter $q_{AB} > 0$ characterizes the catalytic activity. Similarly, the particle might catalyze the reaction $B \rightarrow A$, which we quantify by a parameter $q_{BA} > 0$. Taken together, the boundary conditions at the particle surface then read

$$-j^A(\mathbf{r}_a) = j^B(\mathbf{r}_a) = q_{AB}\phi^A(\mathbf{r}_a) - q_{BA}\phi^B(\mathbf{r}_a), \quad (3)$$

where $j^i(\mathbf{r}_a)$ denote the fluxes normal to the particle surface for $i = A, B$. Note that a passive particle ($q_{AB} = q_{BA} = 0$) imposes no-flux conditions at its boundary. We also impose no-flux conditions at the system boundary, so

Eqs. (1) conserve the average volume fraction $\bar{\phi} = V_{\text{sys}}^{-1} \int (\phi^A + \phi^B) d^3r$ of the components A and B . Here, the integral is over the entire system volume V_{sys} .

The shape of the particle inside the droplet can be described by a superposition of spherical harmonics. The concentration profiles inside and outside the droplet can also be decomposed in spherical harmonics. Since modes with higher degree decay more quickly with the radial coordinate r , deviations from a spherical particle shape are negligible in large droplets. Focusing on this case, we neglect all higher modes of the particle shape and approximate it by a sphere of radius a . Considering this situation in a spherical geometry, we find spherically symmetric stationary solutions of Eqs. (1)–(3) with droplet radii \bar{R} for which the particle is positioned in the geometric center of the droplet.

To investigate the stability of particle positioning and droplet shape, we consider the dynamics of small perturbations. Using a spherical coordinate system (r, θ, φ) centered on the particle, we parametrize the droplet shape $\mathbf{R} = R\mathbf{e}_r$ by the radial distance $R(\theta, \varphi)$. We decompose perturbations of a spherical steady state in terms of real spherical harmonics $Y_l^m(\theta, \varphi)$:

$$R(\theta, \varphi, t) = \bar{R} + \sum_{l=0}^{\infty} \sum_{m=-l}^l \varepsilon_l^m(t) Y_l^m(\theta, \varphi), \quad (4)$$

where $|\varepsilon_l^m| \ll \bar{R}$ are the mode amplitudes. The degree l determines the shape of the perturbation mode, where $l = 0$ corresponds to volume changes, $l = 1$ to translations with respect to the particle at the origin, and all higher l to shape changes. To linear order, the perturbations evolve in time as $\varepsilon_l^m(t) = \varepsilon_l^m(0)e^{\mu_l t}$, where the perturbation growth rates μ_l are independent of m . μ_l can be determined by linearizing Eqs. (1)–(4) [2]. Perturbations with negative μ_l decay in time, and the stationary state with radius \bar{R} is thus stable with respect to such perturbations. Conversely, positive μ_l correspond to unstable perturbation modes.

Particle centering can be analyzed by studying the perturbation modes with $l = 1$. These modes do not change the droplet shape and describe a relative movement of the droplet center with respect to the particle. Figure 1 indicates the interface motion of an asymmetric configuration of particle and droplet characterized by the distribution of droplet material B . The material fluxes implied by the gradients in ϕ^B persist in the stationary state, which is a hallmark of the nonequilibrium conditions introduced by the chemical reactions [16]. Note that the direction of the fluxes depends on the details of the chemical reactions.

We start by analyzing first-order bulk reactions ($k_{AB} > 0$, $k_{BA} > 0$, $k = 0$), where the droplet material B is predominantly produced outside the droplet and diffuses inwards; see Fig. 1(a). In this case, we find $\mu_1 < 0$ for passive particles ($q_{AB} = q_{BA} = 0$), implying that the interface

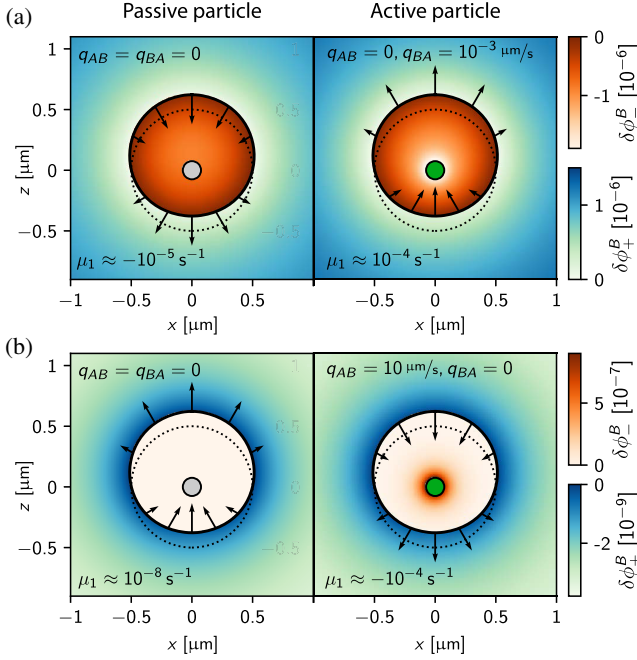


FIG. 1. Behavior of active droplets with displaced particles. Deviatoric volume fractions $\delta\phi_{\pm}^B = \phi^B - \phi_{\pm}^B(\mathbf{R})$ indicate the distribution of droplet material. Shown are first-order reactions [(a); $k_{AB} = 0.01 \text{ s}^{-1}$, $k = 0$] and autocatalytic reactions [(b); $k_{AB} = 0$, $k = 100 \text{ s}^{-1}$] for passive particles (left images) and active particles (right images) with indicated catalytic activities. The remaining model parameters are $V_c = 10^4 \mu\text{m}^3$, $a = 75 \text{ nm}$, $\psi_- = 0.1$, $\psi_+ = 0$, $D = 5 \mu\text{m}^2/\text{s}$, $k_{BA} = 10^{-3} \text{ s}^{-1}$, and $\beta_{\pm} = 10^{-8} \mu\text{m}^2/\text{pN}$ [8]. Additionally, we chose $\varepsilon_1^0 = 0.25 \mu\text{m}$ and adjusted $\bar{\phi}$ such that $\bar{R} = 0.5 \mu\text{m}$. The black arrows indicate the normalized velocity $v\mathbf{n}/|\mu_1|$ of the interface (black solid line) in a reference frame where the particle does not move. In the upper left and lower right panels, the particle is stably positioned in the center of the droplet after relaxation (shown as a dotted line). In the upper right and lower left panels, the state with a centered particle inside the droplet (dotted line) is unstable and the particle is moved off center.

relaxes back to the spherically symmetric state and the central position of the particle is stable. This behavior can be understood by analyzing the fluxes at the droplet surface, which determine the interface dynamics; see Eq. (2). Moving the particle off center brings it closer to one part of the interface, reducing the flux j_-^B of B inside the droplet, since the particle imposes no-flux boundary conditions on the reaction-diffusion system given in Eqs. (1). Conversely, the flux of B outside the droplet is unaffected. Taken together, this leads to a net gain of droplet material at the interface close to the particle, while regions farther away exhibit a net loss. This flux imbalance restores the spherical state and thus centers the particle.

A catalytic activity at the surface of the particle can modify the flux imbalance caused by an off-center position. The imbalance is enhanced when the particle catalyzes the production of droplet material ($q_{AB} > 0$), implying that the

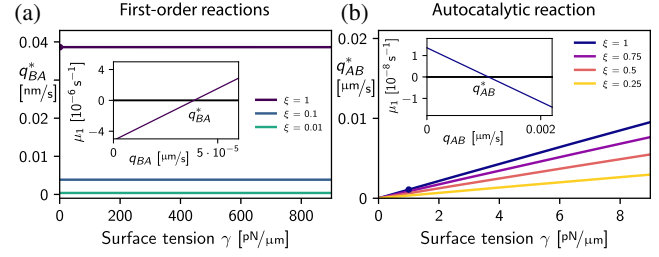


FIG. 2. Critical catalytic rates q_{BA}^* and q_{AB}^* of the particle as a function of surface tension γ for various strengths ξ of the bulk chemical reactions. (a) For first-order bulk reactions ($k_{AB} = \xi \times 10^{-3} \text{ s}^{-1}$, $k = 0$), particles catalyzing $B \rightarrow A$ are centered when $q_{BA} < q_{BA}^*$. (b) For autocatalytic bulk reactions ($k = \xi \times 100 \text{ s}^{-1}$, $k_{AB} = 0$), particles catalyzing $A \rightarrow B$ are centered when $q_{AB} > q_{AB}^*$. (a),(b) The insets show the perturbation growth rates μ_1 as a function of the catalytic rates for parameter values corresponding to Fig. 1 (indicated by the dots in the main panels). Remaining parameters are $k_{BA} = \xi \times 10^{-3} \text{ s}^{-1}$ and given in Fig. 1.

central position is more stable in this case. In contrast, when the particle catalyzes the opposite reaction ($q_{BA} > 0$), the flux imbalance might be reversed, since now droplet material is effectively removed by the particle, which has a stronger influence on closer interfacial regions; see the right panel in Fig. 1(a). In fact, we observe that the central particle position is no longer stable when the catalytic activity q_{BA} exceeds a threshold value q_{BA}^* . Figure 2(a) shows that q_{BA}^* is independent of the surface tension but depends strongly on the overall activity of the chemical reactions in the bulk, emphasizing the nonequilibrium nature. In particular, q_{BA}^* vanishes when chemical reactions are negligible, implying that a passive particle is marginally stable and diffuses freely in a classical passive droplet.

The second class of chemical reactions that we consider are autocatalytic reactions in the bulk ($k_{AB} = 0$, $k_{BA} > 0$, $k > 0$), which account for the dynamics of centrosomes [8]. In this case, droplet material B is predominately produced inside the droplet and exhibits an outwards flux; see Fig. 1(b). The fluxes of A and B are thus oriented opposite to the case of first-order reactions discussed above. Consequently, we find that passive particles ($q_{AB} = q_{BA} = 0$) are not stably positioned in the center of the droplet. Similar to the case of first-order reactions, this instability is amplified if the particle catalyzes the production of precursors ($q_{BA} > 0$). Conversely, we find that a sufficiently strong catalytic activity q_{AB} can stabilize the particle at the geometric center; see the right panel in Fig. 1(b). This behavior can again be understood by analyzing the fluxes at the droplet surface when the particle is positioned off center. At the interface closer to the particle, the material influx due to the chemical conversion at the particle is larger than the efflux away from the droplet, while the efflux dominates the influx at the interface farther away from the particle, causing retraction.

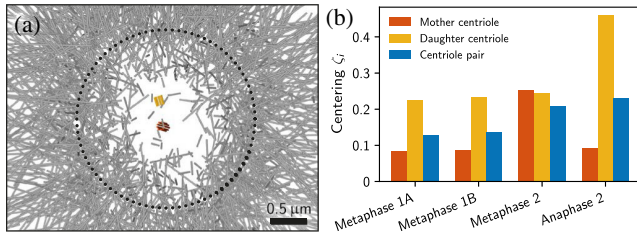


FIG. 3. Experimental data of centrosomes reconstructed from electron tomograms [18]. (a) Representation of the microtubules in a $0.7\text{-}\mu\text{m}$ -thick slice through the centrosome “Metaphase 2.” The microtubules of the mother centriole (red) and its daughter (yellow) are highlighted at the center of the pericentriolar droplet material (indicated by a dotted circle) occupying the central region [20]. (b) Centering coefficients ζ_i of the mother centriole, the daughter centriole, and the centriole pair for the four centrosomes with fully reconstructed centrioles published in Ref. [18].

Taken together, these flux imbalances restore the spherically symmetric state and center the particle. The minimal catalytic activity q_{AB}^* , beyond which the particle is centered in the droplet, decreases for smaller surface tension and weaker chemical reactions; see Fig. 2(b). In particular, q_{AB}^* is typically much smaller than the catalytic activity necessary for guaranteed nucleation of the droplet around the particle [8].

So far, we have not considered the diffusive motion of the particle inside the droplet, which opposes centering. The competition between particle centering by active processes and diffusion can be discussed using an overdamped Langevin dynamics for the particle motion. Here, the diffusivity $D_a = k_B T / \zeta$ is related to the drag coefficient $\zeta = 6\pi\eta a$, which scales with the viscosity η of the droplet. The effect of centering can be represented by a harmonic potential of stiffness $-\frac{1}{2}\zeta\mu_1$ acting on the particle. In the steady state of this simplified picture, the particle position is then normal distributed with variance $\sigma^2 = -D_a/\mu_1$. Consequently, particle centering can be observed when the associated standard deviation is small compared to the droplet radius, $\sigma \ll \bar{R}$.

We can apply our theory to discuss the specific example of centrosome organization. The model parameters for centrosomes have been derived in Ref. [8] and are given in Fig. 1(b). Using the associated growth rate $\mu_1 \approx -10^{-4} \text{ s}^{-1}$ together with the viscosity $\eta \approx 5 \times 10^4 \text{ Pa s}$ estimated for centrosomes [17], we find $\sigma \approx 0.02 \text{ }\mu\text{m}$. This standard deviation is small compared to the typical centrosome size of $\bar{R} \approx 1 \text{ }\mu\text{m}$, so Brownian motion is negligible and our model accounts for centered centrioles under physiological conditions.

In order to investigate the position of centrioles inside centrosomes, we quantified centriole positions using previously published electron tomograms of centrosomes in the one-cell stage of *Caenorhabditis elegans* embryos [18]. Figure 3(a) shows a reconstruction of the microtubules of one mitotic centrosome. Here, centrioles can be identified

by their symmetric arrangement of microtubules around a central tubular structure made of proteins [19]. In particular, the positions of the mother centriole (red) and of its daughter (yellow) can be defined as the center of mass of their microtubules. It is more difficult to define the centrosome center \mathbf{x}_0 . We use the predominant radial orientation of the remaining microtubules to define \mathbf{x}_0 as the focal point of the microtubule axes. The maximum of the associated radial microtubule density profile marks the centrosome radius $R = (1.23 \pm 0.04) \text{ }\mu\text{m}$ (standard deviation, $n = 4$), which is large compared to the centriole length of $(0.22 \pm 0.07) \text{ }\mu\text{m}$. Taken together, we quantify the centriole position by the nondimensional centering coefficient $\zeta_i = |\mathbf{x}_i - \mathbf{x}_0|/R$, where \mathbf{x}_i denotes the position of the mother, its daughter, or the centriole pair. Figure 3(b) shows that both centrioles are typically located close to the center.

An interesting observation is that the mother centriole is often significantly closer to the center than its daughter. Our model can account for this if the mother centriole has a larger catalytic activity than the daughter. In fact, the daughter centriole could be passive and located close to the center, because it is physically tethered to the mother centriole [19,21]. In this case, the particle of radius a in our model would represent only the mother centriole with enzymatic activity q_{AB} . This picture, which neglects effects due to the daughter centriole, is consistent with the fact that the daughter centriole has to mature before it is fully competent to duplicate again [21,22] and that only the mother centriole initiates centrosome growth [23]. The difference in the centriole positioning of mother and daughter thus suggests that this maturation is also required for organizing PCM around the centrioles. For instance, the kinases that mediate the catalytic activity may be recruited only to the fully competent mother centrioles.

In summary, our work shows that particles can be positioned in droplets by material fluxes induced by chemical reactions in the bulk and at the particle surface. Centering of the particle is promoted if droplet material is produced at the particle or outside the droplet. Conversely, the particle is not centered if the material fluxes are reversed when droplet material is produced inside the droplet or degraded at the particle. Particle centering thus depends on the direction of the compositional fluxes created by the chemical reactions.

Compositional fluxes might generally play a role in organizing biological droplets with an internal structure [24]. To describe such systems quantitatively, it will be important to include fluctuations and hydrodynamic effects in the model to account for the dynamics of the small droplets found in biological cells. Moreover, if the droplet size is comparable to the size of an enclosed particle, the particle shape will affect the compositional fluxes and the droplet shape significantly. Conversely, a spherical droplet shape indicates that the shape of the particle is insignificant.

Our work shows that the combination of phase separation with chemical reactions provides detailed control over

the behavior of droplets, which might be exploited in technical applications. For this, it will be important to understand how the compositional fluxes affect the interaction between active droplets and thus the behavior of emulsions of such droplets. Moreover, analyzing this new class of active matter will advance our understanding of nonequilibrium thermodynamics.

D.Z. received funding from the German Research Foundation (DFG) through stipend ZW 222/1-1. J.B., A. A. H., and F. J. acknowledge funding from the European Commission's Seventh Framework Program (FP7/2007-2013) Grant Agreement No. 241548 (MitoSys). T. M.-R. received funding from the Human Frontier Science Program (RGP 0034/2010) and the DFG (Grant No. MU 1423/8-1).

*Corresponding author.

david.zwicker@ds.mpg.de

- [1] D. Zwicker, A. A. Hyman, and F. Jülicher, *Phys. Rev. E* **92**, 012317 (2015).
- [2] D. Zwicker, R. Seyboldt, C. A. Weber, A. A. Hyman, and F. Jülicher, *Nat. Phys.* **13**, 408 (2017).
- [3] C. P. Brangwynne, C. R. Eckmann, D. S. Courson, A. Rybarska, C. Hoegge, J. Gharakhani, F. Jülicher, and A. A. Hyman, *Science* **324**, 1729 (2009).
- [4] A. A. Hyman, C. A. Weber, and F. Jülicher, *Annu. Rev. Cell Dev. Biol.* **30**, 39 (2014).
- [5] D. M. Mitrea and R. W. Kriwacki, *Cell Commun. Signal.* **14**, 1 (2016).
- [6] J. Berry, C. Brangwynne, and M. P. Haataja, *Rep. Prog. Phys.* **81**, 046601 (2018).
- [7] S. Boeynaems, P. Tompa, and L. Van Den Bosch, *Cell Div.* **13**, 1 (2018).
- [8] D. Zwicker, M. Decker, S. Jaensch, A. A. Hyman, and F. Jülicher, *Proc. Natl. Acad. Sci. U.S.A.* **111**, E2636 (2014).
- [9] J. B. Woodruff, O. Wueseke, and A. A. Hyman, *Phil. Trans. R. Soc. B* **369**, 20130459 (2014).
- [10] J. B. Woodruff *et al.*, *Science* **348**, 808 (2015).
- [11] G. D. Gupta and L. Pelletier, *Curr. Biol.* **27**, R836 (2017).
- [12] J. B. Woodruff, B. F. Gomes, P. O. Widlund, J. Mahamid, A. Honigmann, and A. A. Hyman, *Cell* **169**, 1066 (2017).
- [13] O. Wueseke, D. Zwicker, A. Schwager, Y. L. Wong, K. Oegema, F. Jülicher, A. A. Hyman, and J. B. Woodruff, *Biol. Open* **5**, 1431 (2016).
- [14] P. T. Conduit, A. Wainman, and J. W. Raff, *Nat. Rev. Mol. Cell Biol.* **16**, 611 (2015).
- [15] R. Mahen, A. D. Jeyasekharan, N. P. Barry, and A. R. Venkitaraman, *Proc. Natl. Acad. Sci. U.S.A.* **108**, 9310 (2011).
- [16] C. Battle, C. P. Broedersz, N. Fakhri, V. F. Geyer, J. Howard, C. F. Schmidt, and F. C. MacKintosh, *Science* **352**, 604 (2016).
- [17] H. Fantana, Ph.D. thesis, Technische Universität Dresden, 2011.
- [18] S. Redemann, J. Baumgart, N. Lindow, M. Shelley, E. Nazockdast, A. Kratz, S. Prohaska, J. Brugués, S. Fürthauer, and T. Müller-Reichert, *Nat. Commun.* **8**, 15288 (2017).
- [19] M. Winey and E. O'Toole, *Phil. Trans. R. Soc. B* **369**, 20130457 (2014).
- [20] E. O'Toole, G. Greenan, K. I. Lange, M. Srayko, and T. Müller-Reichert, *PLoS One* **7**, e29795 (2012).
- [21] E. A. Nigg and T. Stearns, *Nat. Cell Biol.* **13**, 1154 (2011).
- [22] J. Fu, Z. Lipinszki, H. Rangone, M. Min, C. Mykura, J. Chao-Chu, S. Schneider, N. S. Dzhindzhev, M. Gottardo, M. G. Riparbelli, G. Callaini, and D. M. Glover, *Nat. Cell Biol.* **18**, 87 (2016).
- [23] M. Kirkham, T. Müller-Reichert, K. Oegema, S. W. Grill, and A. A. Hyman, *Cell* **112**, 575 (2003).
- [24] C. P. Brangwynne, T. J. Mitchison, and A. A. Hyman, *Proc. Natl. Acad. Sci. U.S.A.* **108**, 4334 (2011).